Ising model on a Quantum Computer

Giacomo Gasparotto

***Abstract*—In this project we investigate the dynamics of the Transverse-Field Ising Model (TFIM) driven across a quantum phase transition using Matrix Product States (MPS). By mapping the Hamiltonian dynamics onto a quantum circuit, we benchmark the algorithm's scalability, determining the bond dimension requirements to surpass exact diagonalization limits. The simulation captures the breakdown of adiabaticity predicted by the Kibble-Zurek mechanism. Analysis of residual energy, coherent order parameter oscillations, and broadened spin-spin correlations confirms the generation of quasiparticle excitations. Furthermore, the Von Neumann entropy exhibits a continuous growth, tracking the volume-law entanglement production and confirming that the system has evolved into a highly entangled non-equilibrium state.**

I. Introduction

A. *Transverse Field Ising Model*

The Transverse field Ising Model (TFIM) is an exactly solvable model of quantum phase transitions.

It describes the spin interaction on a $1D$ lattice of spins and it is in general represented by the following Hamiltonian:

$$H = -g \sum_i \sigma_i^x - J \sum_i \sigma_i^z \sigma_{i+1}^z \tag{1}$$

where σ_i^x and σ_i^z are Pauli operators acting on qubit i, J is the coupling strength between neighboring spins, and g is the strength of the transverse magnetic field.

The first term introduces quantum fluctuations through the transverse magnetic field, while the second represents classical ferromagnetic interactions [1].

Depending on the dimensionless parameter g/J, the system exhibits two distinct ground-state phases (assuming $J = 1$ from now on):

- $g < 1$ (*Ferromagnetic phase*): the spin-spin interaction dominates, leading to a doubly degenerate ground state where spins spontaneously align along the z-axis;
- $g > 1$ (*Paramagnetic phase*): the transverse field dominates, polarizing all spins along the x-axis and destroying the magnetic order.

At the critical point $g = 1$, the system undergoes a quantum phase transition. Here, the energy gap between the ground state and the first excited state vanishes in the thermodynamic limit, leading to a critical slowing down of the dynamics. Because of this, any finite time evolution across this point breaks the adiabatic approximation, forcing the system into a superposition of excited states [1].

The purpose of this work is to simulate a time-dependent protocol $g(t)$ to investigate how this loss of adiabaticity affects macroscopic observables. Specifically, we expect to observe a residual energy error compared to the exact static ground state, and coherent quantum oscillations in the local magnetization, in accordance with the Kibble-Zurek mechanism [2].

In order to simulate the time evolution of this system we will map it into a quantum circuit and we will solve it exploiting the Matrix Product State (MPS) ansatz of Tensor Networks.

B. *Tensor network approach: MPS ansatz*

The dimension of a quantum many-body Hilbert space scales exponentially with the number of bodies that describes. For instance, in our case, since we are considering qubits, its dimension scales as $\dim(\mathcal{H}) \propto 2^N$ where N is the number of particles.

For large values of N, the simulations of such a system become intractable due to the large computational resources needed. However, physically relevant states often contain less information than the full Hilbert space dimension, allowing for an efficient approximation through data compression techniques.

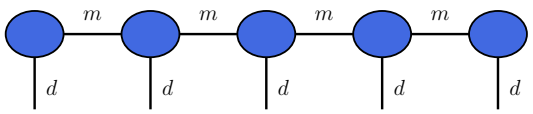

Fig. 1: Sketch of the MPS structure

For that reason, new approaches based on Tensor Networks have been developed. In our case, since we are working with a 1D system, we can exploit the Matrix Product State (MPS) ansatz, which decomposes the quantum state into a chain of local tensors (Fig. 1). In this representation, the complexity of the simulation is reduced to a polynomial scaling: the memory required to store the state theoretically scales as $\mathcal{O}(Nm^2)$, while the computational time required to contract the tensors scales as $\mathcal{O}(Nm^3)$, where m is the maximum allowed bond dimension [3] [4].

The bond dimension m plays a crucial role in determining the accuracy of this approximation, as it limits the maximum amount of entanglement that the ansatz can capture across the spin chain. During the simulation, the application of two-qubit entangling gates (necessary to reproduce the time evolution) naturally tends to increase the entanglement, thus requiring a larger bond dimension to describe the state exactly.

To preserve the polynomial computational cost and prevent the exponential growth of the tensors, a dynamic truncation procedure is performed after the application of these gates.

This is achieved via Singular Value Decomposition (SVD), where only the largest m singular values are kept, while the smallest are discarded. This step introduces a controlled approximation error, the impact of which is analyzed in the III section by studying the convergence of the observables as a function of m.

II. Methods

A. *Circuit mapping*

The time evolution of the TFIM is represented by the following Hamiltonian:

$$H(t) = -g(t)\sum_i \sigma_i^x - \sum_i \sigma_i^z \sigma_{i+1}^z \tag{2}$$

The time dependence appears in the transverse field term, whose strength scales linearly in time as $g(t) = gt/T$, where T is the total protocol time and g the target field strength.

Due to time dependency in Eq. 2, the time evolution operator cannot be written as a single exponential, but we need to consider a time discretization in N steps of the total protocol time T ($dt = T/N$). Thus, the total time evolution operator is represented as the application of short-term evolutions:

$$|\psi(T)\rangle \approx \prod_{k=0}^{N-1} e^{-iH(t_k)dt} |\psi(0)\rangle$$

Within each small time step dt, the Hamiltonian $H(t_k)$ can be considered approximately constant.

The Ising Hamiltonian can be written as a sum of two parts $H(t) = H_{ZZ} + H_X(t)$, but since the two terms do not commute ($[H_{ZZ}, H_X] \neq 0$), we are not able to approximate the time evolution with the usual sum of exponents.

However, if we consider a sufficiently small time step dt for the simulation and accepting to introduce an approximation error ($O(dt^2)$), we can apply the first order Suzuki-Trotter decomposition, which allows us to rewrite the exponential as:

$$e^{-i(H_{ZZ}+H_X)dt} \approx e^{-iH_{ZZ}dt} \cdot e^{-iH_X dt} + O(dt^2)$$

This decomposition is very suitable to be mapped into a quantum circuit simply by using standard rotation gates by mapping the gate rotation angle θ with the actual physical parameters:

- **ZZ-rotation**: $R_{ZZ}(\theta_{ZZ}) = e^{-i\frac{\theta_{ZZ}}{2} Z\otimes Z} \rightarrow \theta_{ZZ} = -2dt$
- **X-rotation**: $R_X(\theta_X) = e^{-i\frac{\theta_X}{2} X} \rightarrow \theta_X = -2g(t)dt$

If the rotation around the x-axis can be simply simulated by the R_X gate, for the R_{ZZ} rotation we have to implement a combination of three gates:

1) CNOT (Control: i, Target: $i+1$) computes the parity;
2) $R_Z(\theta)$ on qubit $i+1$ adds the phase;
3) CNOT (Control: i, Target: $i+1$) uncomputes the parity.

A schematic of the circuit for a single Trotter step is shown in Fig. 2

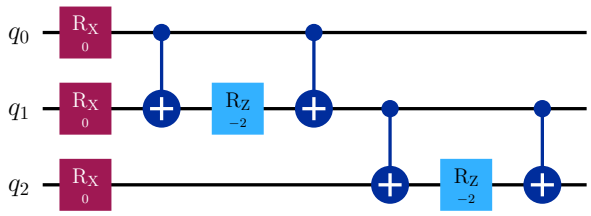

Fig. 2: Representation of one Trotter step of the TFIM for three qubits.

B. *Simulation Framework and Physical Observables*

The quantum circuit was implemented using the `QuantumCircuit` class from the `Qiskit` library [1]. Its execution was then delegated to the Tensor Network backend provided by the `QMatchaTea` and `QTEALeaves` libraries [2]. This approach allows for an efficient handling of the time evolution for systems with many qubits (up to $N = 100$), while keeping the computational complexity bounded through the bond dimension m.

To ensure the reliability of the approximation, a preliminary analysis was performed to study the algorithmic convergence. Specifically, we simulated system sizes ranging from $N = 10$ to 100 qubits, progressively increasing the bond dimension m until the ground state energy density reached a stable plateau. The energy density is defined as:

$$\langle H(t)\rangle/N = -\frac{1}{N}\left(g(t)\sum_i \langle\sigma_i^x\rangle + \sum_i \langle\sigma_i^z\sigma_{i+1}^z\rangle\right) \tag{3}$$

The choice of this specific metric is physically motivated: energy is a two-body observable that obeys the variational principle and is strictly tied to the entanglement of the system. One-body observables, such as local magnetization, can converge prematurely even in approximated states with minimal entanglement, thus providing a false estimate of the overall accuracy of the MPS [4].

Once the optimal bond dimension for our physical purposes and available hardware (Apple M2 CPU) was identified, further analysis was conducted. To verify whether the theoretical expectations outlined in Section I are met, we extracted the following primary macroscopic observables from the contracted tensor network:

- **Ground state energy**: extracted instantaneously to track the breakdown of adiabaticity. By comparing the MPS simulated energy with the exact one, we can quantify the residual excitations generated when driving the system across the quantum critical point;
- **Average magnetization**: the absolute average local magnetization along the z-axis, defined as $M_z = \frac{1}{N}\sum_i |\langle\sigma_i^z\rangle|$, serves as the main order parameter. It allows

[1] https://quantum.cloud.ibm.com/docs/en/api/qiskit/qiskit.circuit.QuantumCircuit
[2] https://www.quantumtea.it

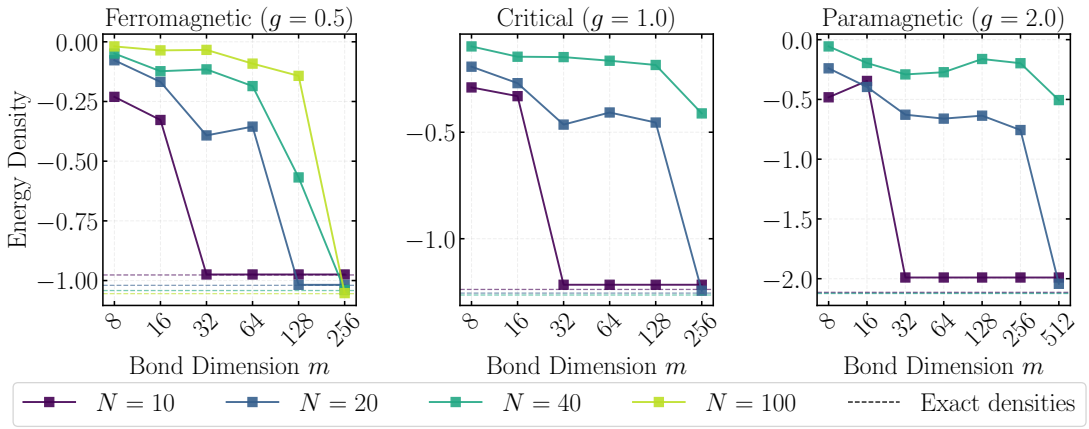

Fig. 3: Bond dimension convergence for different values of g and N.

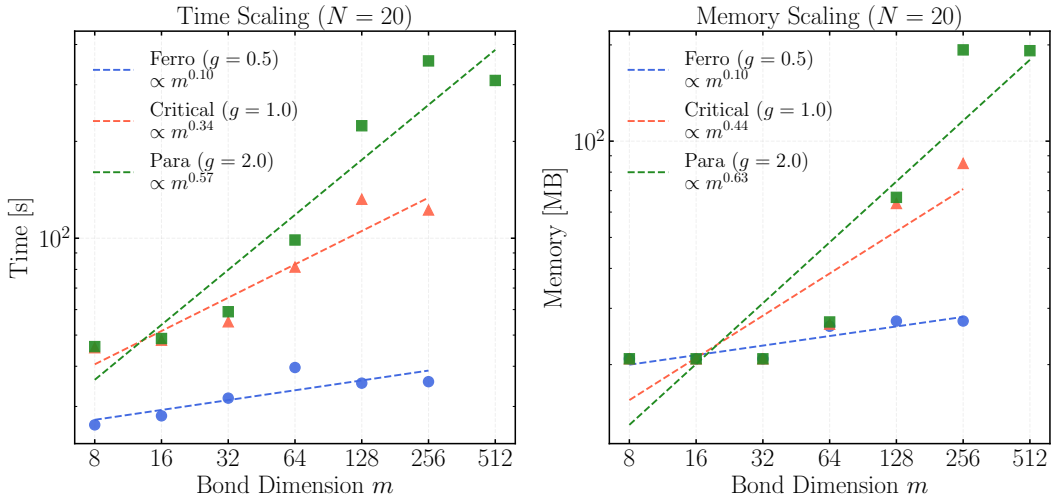

Fig. 4: Time and memory scaling.

us to distinguish between the ordered ferromagnetic phase ($M_z > 0$) and the disordered paramagnetic phase ($M_z = 0$), and visually traces the quantum oscillations induced by the quench dynamics;

- **Spin-spin correlator**: the two-point correlation function, defined as $C(r) = \langle \sigma_i^z \sigma_j^z \rangle$, is computed to study the correlation length of the system. It is expected to show an exponential decay in the ferromagnetic and paramagnetic phases, and a polynomial scaling ($\sim r^{-\eta}$) at the critical point due to scale invariance [5];
- **Von Neumann Entanglement Entropy**: According to Vidal *et al.* [6], the ground-state entanglement entropy of a finite system exhibits a sharp peak at the critical point $g_c = 1$ due to scale invariance. To track the deviation from this adiabatic behavior and quantify the spread of quantum information during the quench, we compute the half-chain bipartite entanglement entropy:

$$S_{N/2} = -\mathrm{Tr}(\rho_A \ln \rho_A) \tag{4}$$

where ρ_A is the reduced density matrix of the first $N/2$ qubits. Using the built-in `TNObsBondEntropy` observable from the `QTeaLeaves` library, this metric allows us to observe the emergence of long-range correlations and volume-law entanglement.

III. Results and Discussion

In this section, we present the outcomes of the Tensor Network simulations of the TFIM.

First, we validate the numerical reliability and efficiency of the MPS ansatz. Then we explore the non-equilibrium behavior of the system through the analysis of macroscopic observables across the critical point.

For all simulations, we set a total protocol time of $T = 40$ and a time step of $dt = 0.05$. These values were chosen to ensure that the system evolves as close to the adiabatic limit as possible, while maintaining a sufficiently small time interval for an accurate Trotter decomposition while being compatible with the available hardware.

Furthermore, to benchmark our results against exact simulations, we are limited by the `StateVector` and exact diagonalization methods, which saturate the hardware memory at $N = 20$ due to the exponential growth of the Hilbert space. For that reason, to compare MPS with exact dynamics, we fixed the system size to $N = 20$ for the physical analysis.

A. *Bond Dimension Convergence and Scaling*

To quantify the impact of the SVD truncation described in Section II, we benchmarked the MPS convergence across the three physical regimes: the *ferromagnetic* phase ($g = 0.5$), the *critical point* ($g = 1.0$), and the *paramagnetic* phase ($g = 2.0$). We evaluated the ground state energy density (Eq. 3) at the end of the adiabatic evolution and compared it against the exact theoretical values.

The convergence results are displayed in Fig. 3. In the ferromagnetic phase ($g = 0.5$), the simulation converges rapidly to the exact value (represented by the dashed horizontal lines) even with low bond dimensions. In contrast, as the transverse field increases ($g \geq 1.0$), reaching convergence becomes more challenging. For the largest system size considered ($N = 40$), the MPS energy density in the paramagnetic phase does not fully converge to the exact value within the explored range of m, indicating that the post-quench state is highly entangled and requires a larger bond dimension to be faithfully represented.

To further characterize the computational cost, we analyzed the time and memory scaling for a fixed system size of $N = 20$, as shown in Fig. 4. Theoretically, the MPS algorithm is expected to scale with a time complexity of $O(Nm^3)$ and a memory complexity of $O(Nm^2)$. However, our numerical results show a deviation from this polynomial behavior. This discrepancy is explained by the saturation of the effective bond dimension. Although the simulation allows for a maximum bond dimension m_{max} (plotted on the x-axis), the SVD truncation automatically reduces the tensor size if the state has low entanglement.

This is clearly visible in the ferromagnetic regime (blue line), where the scaling is nearly flat because the effective bond dimension remains small ($m_{eff} \ll m_{max}$) regardless of the allocated limit. In contrast, in the paramagnetic regime (green line), the scaling slope increases significantly.

B. *Quantum Quench and Kibble-Zurek Dynamics*

To investigate the non-equilibrium dynamics of the system, we simulated a quantum quench across the critical point $g_c = 1$. As anticipated in Section I, while an infinitely slow evolution would perfectly preserve the ground state according to the adiabatic theorem, the closing of the energy gap at $g_c = 1$ leads to a *critical slowing down* [1]. In fact, our finite-rate sweep of the transverse field $g(t)$ forces the breakdown of the adiabatic approximation, triggering the Kibble-Zurek mechanism [2].

This theoretical prediction is confirmed by the data in Figs. 5 and 6.

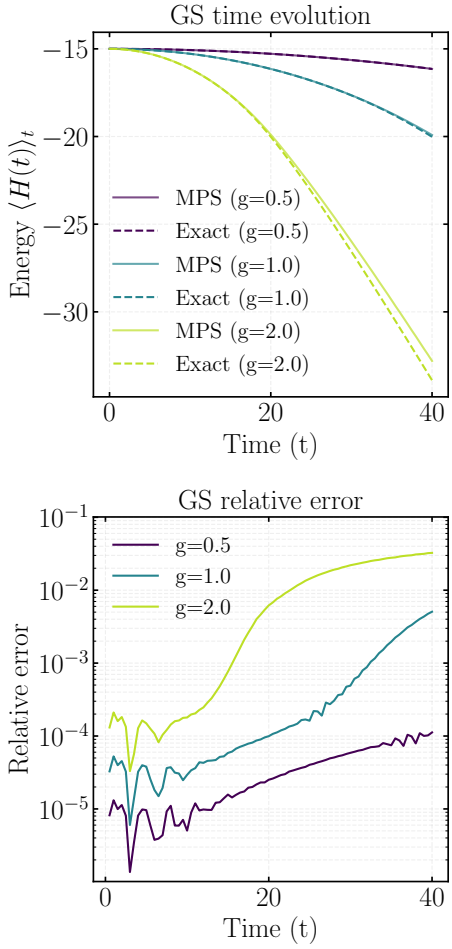

Fig. 5: Ground state energy comparison between MPS calculation and exact diagonalization in time. The relative errors are displayed in the bottom panel.

Figure 5 compares the time evolution of the ground state energy computed via MPS with the exact instantaneous ground state energy. While the MPS perfectly tracks the exact energy in the ferromagnetic phase ($g = 0.5$), a clear deviation emerges as the system approaches the critical point ($g = 1.0$) and enters the paramagnetic phase ($g = 2.0$). This residual energy confirms that the system has absorbed excitations and is no longer in its true ground state.

The macroscopic consequences of these excitations are perfectly captured by the average magnetization dynamics, shown in Fig. 6.

The upper panel displays the order parameter as a function of the transverse field strength g. The MPS closely follows the exact static ground state only up to the critical point $g_c = 1$, after which it deviates from the exact curve, showing heavy fluctuations.

The bottom panel of Fig. 6 provides a spatial representation of this phenomenon through a heatmap of the local magnetization $\langle \sigma_i^z \rangle$. After crossing the phase transition, the heatmap does not become homogeneously dark (which would represent

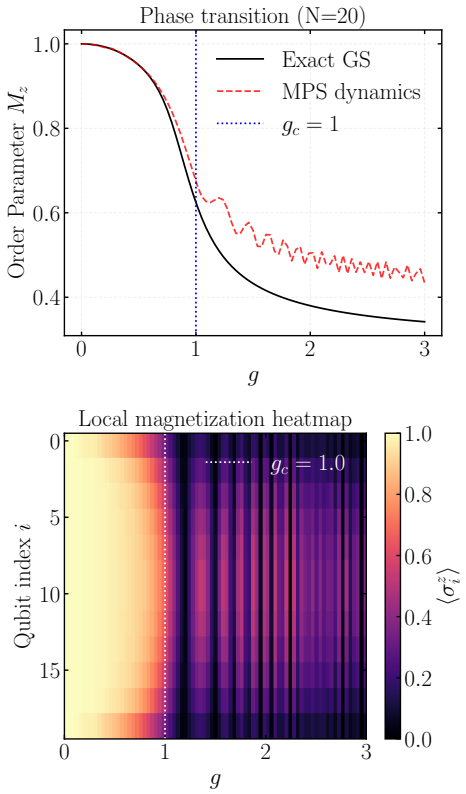

Fig. 6: Comparison of the order parameter compared to the exact simulation. The local magnetization heatmap displays the same behavior than the top panel.

the true paramagnetic ground state with zero z-magnetization). Instead, we observe distinct alternating vertical stripes.

Since the transverse field g is linearly proportional to the simulation time ($g \propto t$), these stripes represent quantum oscillations in time. Because the system was forced into a superposition of excited states at the critical point, the different components of the wavefunction evolve with different phase factors ($e^{-iE_n t}$). This causes the magnetization of the qubits to "pulse" synchronously. The fact that these oscillations do not immediately dephase is a direct consequence of the finite-size nature of our system ($N = 20$), providing a visual confirmation of the coherent non-equilibrium dynamics induced by the quantum phase transition [5].

Furthermore, the heatmap illustrates the spatial inhomogeneities introduced by the Open Boundary Conditions (OBC). As visible in the top and bottom rows of the bottom panel, the boundary spins ($i = 0$ and $i = N - 1$) lose their ferromagnetic order significantly earlier than the bulk spins ($g \approx 0.6$). This finite-size effect occurs because the boundary qubits have one neighbor instead of two, making their local z-interactions weaker.

C. *Spin-spin correlation*

Another relevant observable to characterize the phase transition is the spatial correlation matrix $|\langle \sigma_i^z \sigma_j^z \rangle|$. In Fig. 7, we display the global spatial structure of the system across the three regimes.

The first panel shows the ferromagnetic phase ($g = 0.5$). Here, the z-interaction term is predominant, establishing a strong long-range order where all spins remain highly correlated. As already discussed in Section III-B, the corners of the matrix appear darker. This is a direct consequence of the open boundary conditions of the chain.

The situation changes drastically in the paramagnetic case ($g = 2.0$), displayed in the third panel. In this regime, the transverse field dominates and the macroscopic z-ordering is destroyed, leading to a rapid decay of correlations between qubits, which appear strictly confined to the main diagonal.

The central panel ($g_c = 1$) captures the critical behavior and the effects of the Kibble-Zurek mechanism [2]. As the system approaches the phase transition, the closing of the energy gap leads to the critical slowing down. The system is no longer able to adapt adiabatically to the time-evolving Hamiltonian. Unlike the exponential decay ($C(r) \sim e^{-r/\xi}$) of the paramagnetic phase, the critical correlations persist over longer distances following an algebraic decay ($C(r) \sim r^{-\eta}$). This results in a significant "diffused" broadening of the correlation band visible in the heatmap, distinguishing the critical state from the sharp localization of the paramagnetic regime [5].

D. *Von Neumann Entanglement Entropy*

Finally, we analyze the bipartite Von Neumann entropy $S_{N/2}$ to quantify the spread of quantum information. The results are shown in Fig. 8.

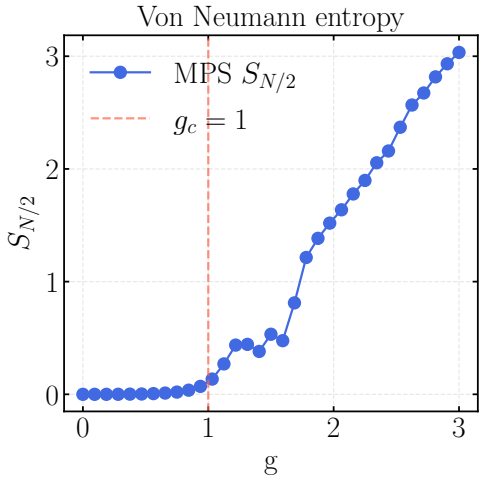

Fig. 8: Evolution of the half-chain Von Neumann entropy $S_{N/2}$ as a function of the transverse field $g(t)$. The vertical dashed line marks the critical point $g_c = 1$.

In a purely adiabatic scenario, we theoretically expect a sharp peak exactly at the critical point ($g_c = 1$), followed by a rapid decay to zero in the paramagnetic phase.

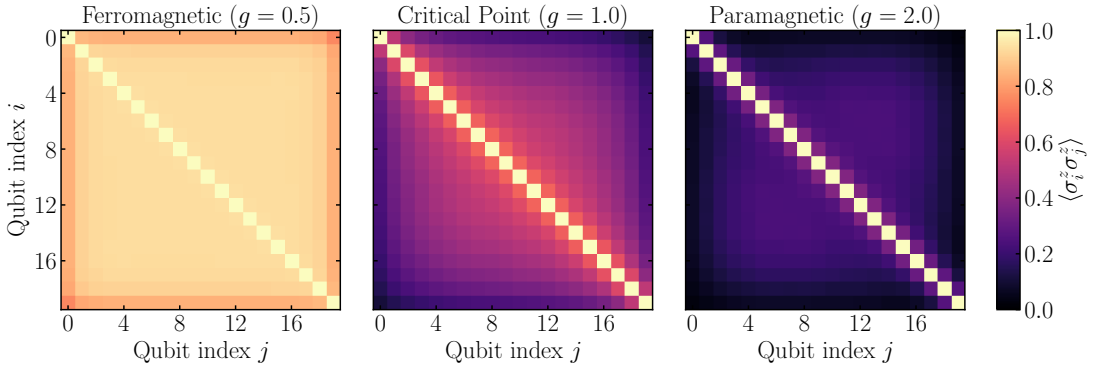

Fig. 7: Full spatial correlation matrices $|\langle \sigma_i^z \sigma_j^z \rangle|$ for $N = 20$.

However, our dynamical simulation reveals a different behavior. In the ferromagnetic phase ($g < 1$), the entropy remains low. As the system crosses the critical region, $S_{N/2}$ increases linearly, consistent with the predictions for quantum quenches [7]. In the paramagnetic phase ($g > 1$), the entropy does not decay but keeps growing tracking the volume-law entanglement production [7].

This growth is again a signature of the non-equilibrium dynamics driven by the Kibble-Zurek mechanism. The breakdown of adiabaticity at the critical point pumps the system into a highly excited state populated by entangled quasiparticles. These excitations propagate coherently and reflect off the boundaries, preventing the system from relaxing to the low-entropy ground state [2].

IV. Conclusion

In this work, we investigated the time evolution of the Transverse Field Ising Model (TFIM) by mapping the system onto a quantum circuit architecture and simulating its dynamics using the Matrix Product State (MPS) ansatz within the Tensor Network framework.

A primary focus of our analysis was the scalability of the algorithm compared to classical state-vector methods. Although exact diagonalization techniques are typically limited to system sizes of $N \approx 20$ due to the exponential growth of the Hilbert space, our MPS implementation successfully simulated time evolutions up to $N = 100$ qubits, with performance constrained only by the simulation time and available memory.

Physically, the time-dependent simulation revealed the out-of-equilibrium dynamics that emerge when a system is driven across a quantum phase transition. This behavior is consistent with the Kibble-Zurek mechanism, which predicts that the breakdown of adiabaticity near the critical point, caused by the closing of the energy gap, leads to the generation of quasiparticle excitations.

To verify this mechanism, we analyzed several macroscopic observables, all of which confirmed the theoretical expectations:

- The **total energy** of the system deviated significantly from the instantaneous ground state energy after the critical point, quantifying the residual excitation energy injected by the quench;
- The **local magnetization** exhibited coherent oscillations in the paramagnetic phase, a direct signature of the quasiparticles generated at the critical point;
- The **spin-spin correlation matrices** revealed a "broadening" of the correlations, proving that the system retains correlations over longer distances than adiabatically expected due to the critical slowing down;
- Finally, the **Von Neumann entropy** showed a continuous, rapid growth rather than decaying, confirming that the system has permanently left the low-entropy ground state.

In conclusion, this project demonstrates that Tensor Networks are not only a powerful computational tool for overcoming the limits of classical simulation but also provide a robust framework for exploring complex non-equilibrium phenomena in many-body quantum systems.

References

[1] J. Dziarmaga, "Dynamics of a quantum phase transition: Exact solution of the quantum ising model," *Physical review letters*, vol. 95, no. 24, p. 245701, 2005.

[2] W. H. Zurek, U. Dorner, and P. Zoller, "Dynamics of a quantum phase transition," *Physical review letters*, vol. 95, no. 10, p. 105701, 2005.

[3] S. Montangero, *Introduction to Tensor Network Methods: Numerical Simulations of Low-Dimensional Many-Body Quantum Systems*. Cham: Springer, 2018.

[4] U. Schollwöck, "The density-matrix renormalization group in the age of matrix product states," *Annals of physics*, vol. 326, no. 1, pp. 96–192, 2011.

[5] P. Calabrese, F. H. Essler, and M. Fagotti, "Quantum quench in the transverse-field ising chain," *Physical review letters*, vol. 106, no. 22, p. 227203, 2011.

[6] G. Vidal, J. I. Latorre, E. Rico, and A. Kitaev, "Entanglement in quantum critical phenomena," *Physical review letters*, vol. 90, no. 22, p. 227902, 2003.

[7] P. Calabrese and J. Cardy, "Evolution of entanglement entropy in one-dimensional systems," *Journal of Statistical Mechanics: Theory and Experiment*, vol. 2005, no. 04, p. P04010, 2005.